Review of Scientific Instruments

3D printed nozzles on a silicon fluidic chip

Cite as: Rev. Sci. Instrum. **90**, 035108 (2019); https://doi.org/10.1063/1.5080428
Submitted: 08 November 2018 . Accepted: 26 February 2019 . Published Online: 20 March 2019

Sven Bohne, Michael Heymann, Henry N. Chapman, Hoc Khiem Trieu, and Saša Bajt

View Online Export Citation CrossMark

ARTICLES YOU MAY BE INTERESTED IN

A high speed X-Y nanopositioner with integrated optical motion sensing
Review of Scientific Instruments **90**, 035002 (2019); https://doi.org/10.1063/1.5055715

Improved gating device of time-of-flight ion mass analyzer for ion sources
Review of Scientific Instruments **90**, 033305 (2019); https://doi.org/10.1063/1.5088576

Piezospectroscopic measurement of high-frequency vibrations in a pulse-tube cryostat
Review of Scientific Instruments **90**, 034901 (2019); https://doi.org/10.1063/1.5080086

Lock-in Amplifiers up to 600 MHz
starting at $6,210

Zurich Instruments
Watch the Video

© 2019 Author(s).

Review of Scientific Instruments ARTICLE scitation.org/journal/rsi

3D printed nozzles on a silicon fluidic chip

Cite as: Rev. Sci. Instrum. 90, 035108 (2019); doi: 10.1063/1.5080428
Submitted: 8 November 2018 • Accepted: 26 February 2019 •
Published Online: 20 March 2019

View Online Export Citation CrossMark

Sven Bohne,[1,a)] Michael Heymann,[2,a)] Henry N. Chapman,[3,4,5] Hoc Khiem Trieu,[1] and Saša Bajt[6,b)]

AFFILIATIONS

[1]Hamburg University of Technology, Eissendorfer Str. 42, 21073 Hamburg, Germany
[2]Max-Planck-Institute of Biochemistry, Am Klopferspitz 18, 82152 Martinsried, Germany
[3]Center for Free Electron Laser Science, Notkestrasse 85, 22607 Hamburg, Germany
[4]Department of Physics, University of Hamburg, Luruper Chaussee 149, 22607 Hamburg, Germany
[5]Centre for Ultrafast Imaging, Luruper Chaussee 149, 22607 Hamburg, Germany
[6]Deutsches Elektronen-Synchrotron DESY, Notkestrasse 85, Building 99, 22607 Hamburg, Germany

[a)]**Contributions:** S. Bohne and M. Heymann contributed equally to this work.
[b)]**Author to whom correspondence should be addressed:** sasa.bajt@desy.de

ABSTRACT

Serial femtosecond crystallography is a new method for protein structure determination utilizing intense and destructive X-ray pulses generated by free-electron lasers. The approach requires the means to deliver hydrated protein crystals to a focused X-ray beam and replenish them at the repetition rate of the pulses. A liquid-jet sample delivery system where a gas dynamic virtual nozzle is printed directly on a silicon-glass microfluidic chip using a 2-photon-polymerization 3D printing process is implemented. This allows for rapid prototyping and high-precision production of nozzles to suit the characteristics of a particular sample and opens up the possibility for high-throughput and versatile sample delivery systems that can integrate microfluidic components for sample detection, characterisation, or control. With the hybrid system described here, stable liquid jets with diameters between 1.5 μm at liquid flow rate of 1.5 μl/min and more than 20 μm at liquid flow rate of 100 μl/min under atmospheric and vacuum conditions are generated. The combination of 2D lithography with direct 3D printing may streamline the integration of free-form-features and also facilitate scale-up production of such integrated microfluidic devices that may be useful in many other applications such as flow cytometry and optofluidics.

© 2019 Author(s). All article content, except where otherwise noted, is licensed under a Creative Commons Attribution (CC BY) license (http://creativecommons.org/licenses/by/4.0/). https://doi.org/10.1063/1.5080428

I. INTRODUCTION

Serial femtosecond crystallography (SFX) utilizing intense pulses from an X-ray Free Electron Laser (XFEL) is becoming an established technique for the measurement of protein structure and dynamics, particularly for hard to crystallize proteins.[1] Intense XFEL pulses of short enough femtosecond duration allow exposures that are vastly greater than tolerable at conventional sources by generating a diffraction pattern before the pulse destroys the sample.[2] Each sample can therefore only contribute to a single two-dimensional diffraction pattern. The complete three-dimensional diffraction dataset must be assembled from many thousands of snapshots from crystals in various orientations. It is thus very important that the protein crystals are quickly replenished to efficiently record the dataset at the rate that pulses are created, which ranges from 120 Hz at the Linac Coherent Light Source (SLAC, USA) to megahertz rates at the European XFEL (Hamburg, Germany). Liquid microjets provide the necessary velocities to do this, keep protein microcrystals stable in liquid (the crystallization buffer), and generate a tolerably low background to the diffraction pattern (proportional to the jet thickness). The intersection of the intense x-ray beam with the flowing sample is usually in the continuous liquid jet, prior to its breakup into drops.[1] To minimize background, the interaction with the beam is often in a vacuum environment. This is possible by flow focusing of the jet with gas, using a so-called gas dynamic virtual nozzle (GDVN).[3–5] The gas also helps to prevent cooling of the liquid in the vacuum chamber although the time that a crystal flows in the free jet prior to

© Author(s) 2019

the X-ray exposure is much shorter than 1 ms.[6] The optimized design of flow-focused nozzles is critical to obtain jets of the requisite small diameter (less than several micrometers), sufficient length (ideally >100 μm), with high temporal and spatial stability over the duration of the measurement (possibly many hours). For low-frequency X-ray sources, such as those operating at 120 Hz, sample consumption can be reduced by reducing the liquid flow rate, which requires nozzles of high perfection. The recent invention of double flow-focused nozzles, which introduce the sample suspension into a jet-forming sheath liquid, has allowed efficient data collection at a sample consumption of about 3 μl/min.[7] Much of the recent progress in the design and operation of microjets can be attributed to the introduction of high-resolution 3D printing of nozzles, which gave the necessary precision of alignment and symmetry of the liquid and gas orifices.[8] 3D printed nozzles with improved design were recently also successfully used in experiments at the European XFEL.[9]

Two-photon-polymerization (2-pp) allows printing of 3D polymer structures with a resolution down to 0.2 μm.[10] The design freedom offered by 3D printing enables novel nozzle geometries such as needed for mixing of sample with a reactant prior to X-ray measurement, multiplexing multiple nozzles for quickly changing nozzle parameters, or integrating diagnostics or sensors into the sample injection system.[11] To benefit from the high-resolution 3D printing but to avoid printing large structures that, in their entirety, do not require such high precision, we combined high-resolution 3D printing of the nozzle tip with microfluidic technology. We can benefit from extensive developments in microfluidic technologies based on soft or optical lithography on planar silicon and glass.[12–14] Previous successful demonstrations that combined 3D printing with lithographic microfluidics included 3D enzyme reactors in polydimethylsiloxane chips, microsieves in microglass channels, acoustic micromixers in a silicon glass chip, and direct printed structures in microfluidic channels to filter particles and cells by size and morphology.[15–20]

Lithographically prepared microfluidic platforms permit integration of smart components that can sense and control liquid streams and enable fast switching between them. They also support designs of multiplexed nozzles with on-chip switching and sorting of samples, as well as fast and low-cost mass production. One can envision that combining micro-electro-mechanical systems (MEMS) technologies with high resolution 3D printed nozzles will also facilitate controlled mixing to study fast chemical reactions with short pulsed x-ray sources. In addition, the direct printing of 3D nozzles (volumes of only about 1 mm^3) onto such a platform simplifies the connection to the microfluidic chip.

In this paper, we describe the direct printing of a GDVN nozzle onto an etched silicon and glass chip. The silicon and glass provide the fluidic chip platform, which we refer to as the silicon glass interface chip (SGIC). Microfluidic channels with a high aspect ratio are etched into the silicon via deep reactive ion etching (DRIE). Glass is used as a lid to seal fluidic structures and/or as a fluidic connection to the lab equipment. The nozzles prepared this way were tested using typical values of gas and liquid pressures and flows to obtain liquid jets with properties desired in SFX experiments. The tests were performed with pure water and suspensions of protein crystals such as granulovirus and lysozyme crystals dispersed in liquid buffers.[7,21,22]

II. RESULTS AND DISCUSSION

A. Design and fabrication of the SGIC

A 3D rendering of the nozzle and chip assembly is shown in Fig. 1(a). The SGIC is prepared such that all inlet capillaries connect on one side. In this work, we fabricated three inlet channels (such as would be needed for a double flow-focus nozzle, for example).[7] In our experiments, we only use two of these, one as a gas line and one as a liquid line. These inlets connect the nozzle with the necessary lab equipment for supplying the sample and gas, for example, syringe pumps and a pressurized gas source. The nozzle is printed directly onto the SGIC, on the side opposite to the inlets. The SGIC is prepared by combining two wafers structured by photolithography. The two wafers, one glass and one silicon, act as a sandwich that houses the inlet capillaries, which connect in the plane of the wafers, as depicted in Fig. 1(b). The sandwich also creates the sealed microfluidic channels to connect the capillaries to the nozzle. The nozzle is attached to the outside face of the silicon and oriented to the jet away from the chip in a direction

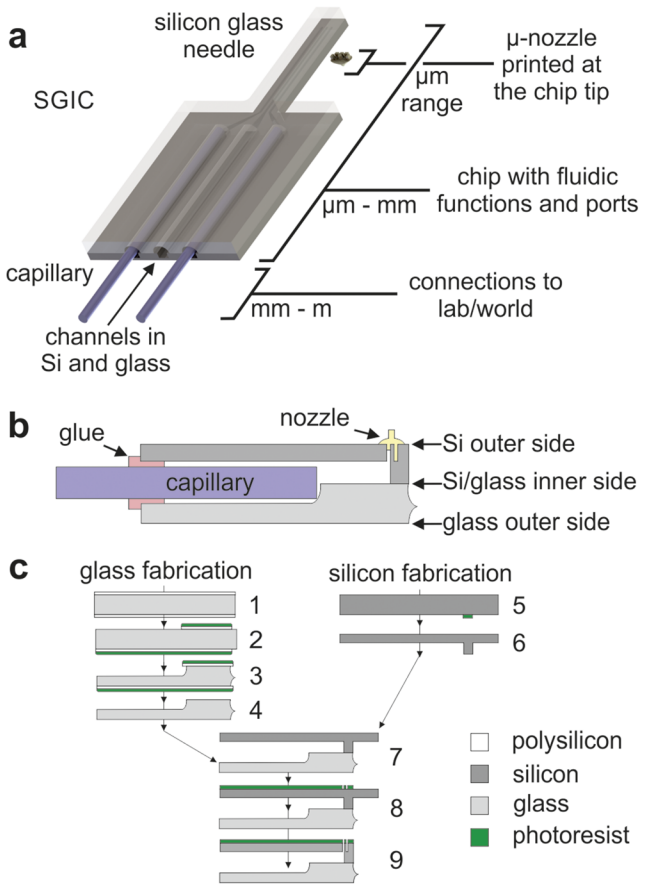

FIG. 1. Silicon glass interface chip design: (a) 3D rendering of the developed SGIC, shown here with two inlet capillaries. (b) Side view schematic of the assembled SGIC with the printed nozzle and glued capillary. (c) Schematic of the fabrication process with individual steps (1-9) described in the text.

© Author(s) 2019

perpendicular to the face. Excess silicon and glass close to the nozzle is removed completely to form a silicon glass "needle." This is required for using the nozzle in diffraction experiments to ensure that the wafer material does not shadow the X-ray diffraction of samples.

To fabricate the SGIC [Fig. 1(c)], a thin polysilicon layer was deposited onto both sides of a 500 μm thick borosilicate glass wafer using a low-pressure chemical-vapor deposition process to promote photoresist adhesion and to serve as a hard mask for the subsequent etching of the glass wafer (step 1). Both sides of this wafer were then spin-coated with a thin film of AZ9260 (Microchemicals) photoresist, which was then exposed to a photomask and developed in 1% NaOH (step 2). The polysilicon under the exposed and developed features was then stripped by etching with SF6 plasma, and the wafer was then wet etched in 49% HF acid for 60 min (step 3). Unmasking of the borosilicate glass on both sides resulted in complete dissolution of the glass and was used to shape the needle section near the 3D printed nozzle tip. Alternatively, only the inside surface of the glass wafer was etched, to yield channels with a semicircular profile of 250 μm radius to provide connection ports for the inlet capillaries. Photoresist and polysilicon were then removed (step 4). The second half of the SGIC was made from a 325 μm thick double side polished silicon wafer that was structured anisotropically by a two-stage DRIE (deep reactive-ion etching). First, the inner side of the silicon [facing downwards in the diagram of Fig. 1(b)] was etched (steps 5 and 6). This step etched the 170 μm deep channels with a rectangular profile (for fluid and gas delivery) and also the contours for the needle. The channels were 400 μm wide in the position where the inlet capillaries attach and were designed to match up with the etched semicircular channels in the glass. Beyond the insertion position of the inlet capillaries, the etched channels in the silicon narrowed down to a width of 100 μm for interfacing with the 3D printed nozzle on the other side of the silicon.

The glass and silicon wafer were bonded by an anodic bonding process (step 7). This created the inner sides of silicon and glass seen in Fig. 1(b). Photoresist was applied to the outer silicon side, and the mask was aligned to the structures on the rear via infrared (IR) imaging prior to exposure and developing (step 8). A second DRIE was performed on the outer silicon side of the bonded substrate (step 9). The photomask included tunnels, which were etched 155 μm through the remaining thickness of the silicon to connect with the channels on the other side. These provided the fluidic and gas connections to the 3D printed nozzle. The mask design accounted also for complete removal of silicon to obtain the final needle shape. In the same process, 155 μm deep wells were etched in the outer side of the silicon to provide structures for adhesion between the printed material of the nozzle and the silicon. Additionally, geometric structures to align the 3D prints to the silicon structures were included. After photoresist removal, the glass-silicon wafer was diced to obtain individual SGICs. The final dimensions of SGIC were 6.25 mm × 12.5 mm × 0.825 mm, with a needle of 1.0 mm × 0.8 mm. Different needle lengths were designed and tested to find the optimum length that is still mechanically stable during the dicing process. Functional needles as long as 5.0 mm were produced. In addition to the chips with individual SGIC structures, chips with an array of 8 SGICs were fabricated on the same wafer. This allowed for faster printing, developing, and testing of the nozzles. Finally, a nozzle tip was printed directly on the SGIC.

B. Design of 3D printed nozzles

In proof-of-principle experiments, Nelson *et al.*[8] demonstrated that 2-pp 3D printed GDVNs are suitable for SFX sample delivery. However, by directly adapting a design of a standard glass capillary GDVN, their design inherited jetting performance and assembly limitations.[8] Through extensive testing, we improved on the initial design of Nelson *et al.*[8] by reducing all critical nozzle dimensions by about a factor of two [Fig. 2(a)]. Since smaller nozzle volumes print proportionally faster, this allowed for about 10-fold increase in production rates. More importantly, smaller gas and liquid apertures are able to form stable jets at lower flow rates, hence allowing the reduction in sample consumption rates, a highly valuable characteristic in SFX.[23] The nozzle body design used here is basically the same as the nozzle design used by Wiedorn *et al.*[9] [Fig. 2(b)] except for the orifice shape. However, directly printing the nozzle on the microfluidic chip, as presented in this work, greatly simplifies nozzle assembly. In particular, it eliminates the gluing of the nozzle tip to the capillaries, a step that often causes misalignment, leaks, and step features in the fluid channels that may cause clogging. In previous work,[8,9] nozzles were first printed on flat glass substrates coated with indium tin oxide (ITO). After printing, they had to be separated from the glass, developed [in 1-methoxy-2-propanyl acetate (PGMEA)], and finally attached to the gas and liquid capillaries with glue. Here a nozzle tip was printed directly to a microfluidic chip with no need for direct gluing of the nozzle tip to the capillaries. The chip serves as a manifold for attaching the capillaries that deliver the gas and liquids.

Details on how we modified the design of the main nozzle body section to reroute gas and liquid supplies from the concentric arrangement in the nozzle tip to the separate parallel lines of the SGIC chip are shown in Fig. 2(b). Also, a strong and gas-tight attachment of the nozzle to the chip is required to withstand the 1×10^5 Pa–3×10^5 Pa liquid and gas pressures encountered in routine SFX sample delivery.

To strengthen the nozzle attachment, we etched dedicated structures into the silicon chip. These were filled with the photoresist material during printing. Such anchor structures, which we refer to as "roots," greatly reduced nozzle detachment during operation. The root structures are fully printed structures which fill the dedicated holes in the silicon. This increases the mechanical bonding strength between printed material and silicon, by giving something for the printed object to grip, like the roots of a tree. Additional "seal" structures are implemented at the fluidic transition from the silicon outlet to nozzle inlet. Each sealing structure is a hollow cylindrical shell or "pipe" which is printed into the circular opening in the silicon chip and which continues the liquid or gas line from the nozzle body to make a tight connection to the channels in the SGIC. The connections operate like ring gaskets. The slight expansion of the printed material in the development process generates a force that presses the flexible printed material to the surrounding silicon.

The complete nozzle design was prepared with Solidworks™ and consists of three integrated components: the nozzle tip with orifice, the main body for fluid contacting, and the root and seal structures to connect the printed material to the silicon [Fig. 2(b)]. Although all three components are printed as one single structure, they are shown separately in Fig. 2(b) to highlight their different

© Author(s) 2019

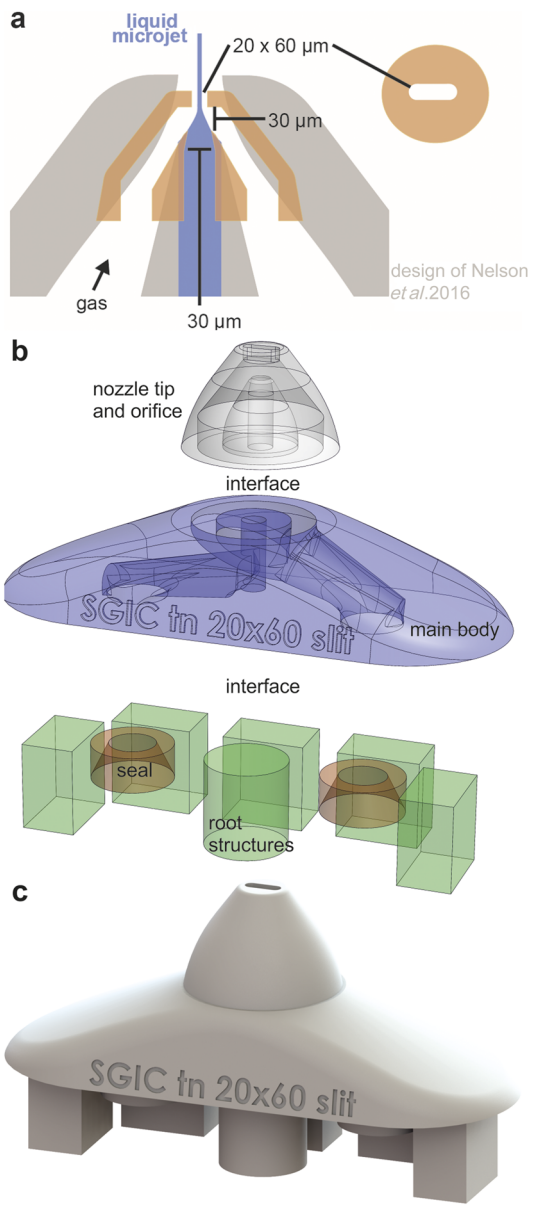

FIG. 2. 3D printed nozzle design: (a) Schematic of the used GDVN nozzle tip (orange brown) is overlayed by the design of Nelson *et al.* indicated in gray brown.[8] There is a major difference in the overall nozzle size and orifice shape and dimension. The nozzle orifice is a slit hole, with dimensions of 20 μm × 60 μm. The inner liquid capillary diameter is 30 μm, and the distance between the tip of the liquid capillary and the nozzle orifice is 30 μm. The liquid jet is indicated in blue. The nozzle tip design is similar to the one successfully used in experiments at the European XFEL[9] except in that case the nozzle orifice was a 50 μm diameter circular hole. (b) The three independent components of the nozzle: nozzle tip and orifice, main body with fluid channels, and root and seal structures, which help to connect the printed material to the silicon. To produce nozzles with different jet properties, only the design of the nozzle tip and orifice have to be modified. The root and seal structures are important for the adhesion and sealing to the Si-glass chip, while the main body guides the fluid streams from a linear to a co-axial arrangement. (c) The complete design with two inlets for liquid and gas and roots and seals at the bottom of the main structure.

functions and modular design. These various parts of the structure can be easily modified to achieve designs that can be created and tested rapidly. Our GDVN design uses two of the three SGIC channels, and the middle fluidic channel was filled with an additional root structure. The main body and the root and seal structure fit to the silicon chip dimensions. All results shown in this paper were obtained from nozzles with these dimensions [Fig. 2(c)].

C. Direct printing on silicon

The nozzle geometry was exported to Standard Triangulation/Tesselation Language format and converted to a 3D print job using DeScribe and Nanowrite software (Nanoscribe GmbH, Karlsruhe, Germany).[10] Several nozzles were printed on SGICs using a 25× dip-in laser lithography (DILL) objective. The IP-S resist (Nanoscribe GmbH, Karlsruhe, Germany) was used for all nozzles described here, due to its excellent performance in previous 3D printed nozzles.[8,9] This high viscosity negative photoresist was designed for mesoscale printing in DILL-configuration, can be used without baking, and has minimum shrinkage.[10]

While 2-pp printing on glass is a standard procedure of the Nanoscribe instrument, direct printing on silicon requires additional sample preparation.[15–20] We fabricated a custom sample holder to position the SGIC substrate in the 2-pp printer. For standard 2-pp printing, clean unstructured glass slides are readily available. As we determined, ensuring sufficiently clean silicon chips is critical for successful printing. This is hard to realize because of many fabrication steps in the preparation of SGIC substrates. Our cleaning procedure included washing silicon chips with acetone, isopropanol, and water. Since silicon is more reflective than glass, it required a reduction in the laser power for printing as compared to the power used with the glass substrate. Excessive laser power causes microexplosions of overexposed resists and destroys the printed structure. During the printing process, the focused laser beam was scanned in a 3D raster trajectory in the resist, beginning from the bottom. Initializing the start of this exposure scan with the focus located below the silicon surface by several micrometers increases the bonding between the resist and the silicon.[10,17] We started the scan at a position 100 μm below the silicon surface to form the anchor structures in the etched root and seal volumes below. Both root and seal structures in the 3D nozzle design were oversized in width relative to the cavities in the silicon. With this adjustment, we found a crude alignment to about 10 μm precision to be sufficient as the oversized features ensured the whole root cavity in SGIC to become fully polymerized reliably.

To start the printing process, a small drop of the IP-S resist was placed on the clean silicon surface of the SGIC. Alignment structures on the silicon surface, and visible with the CCD camera attached to the 2-pp printer, were used to achieve the necessary alignment precision. Stages moving the array chip in two orthogonal horizontal directions and rotating it in the horizontal plane allowed automated printing of several nozzles per chip, allowing us to print up to 8 nozzles per batch. Figure 3(a) displays an image of one nozzle in the middle of the printing process.

In addition to optimizing the laser exposure protocol, it was challenging to develop the printed material. A passive development in PGMEA for several days was used, with a daily PGMEA exchange. Due to the SGIC form, the PGMEA had to diffuse through the millimeter-long fluidic channels to reach the nozzle's back side to

© Author(s) 2019

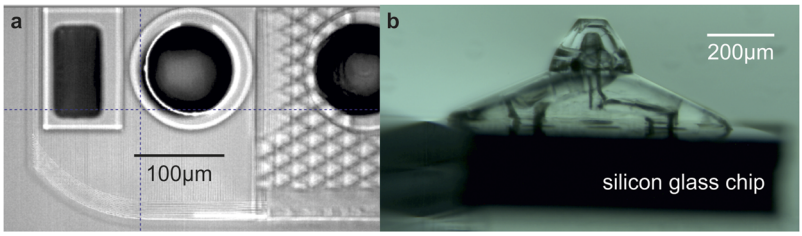

FIG. 3. SFX nozzle printed on SGIC: (a) A view from the top of the nozzle in the middle of the printing process, as imaged with the Nanoscribe camera. The rectangular roots and the circular seal structures are visible. (b) An optical microscope image of a printed nozzle on the silicon glass needle (side view). The nozzle is 850 μm wide, 350 μm high, and 310 μm deep. The internal liquid guidance channels are visible. The root and seal structures are burrowed into the silicon.

dissolve the unexposed material of the nozzle's channels. Figure 3(b) shows a microscopic image of a printed nozzle with developed and unobstructed inner liquid channels achieved with this development procedure.

D. Final nozzle assembly and jet characterization setup

The final assembly step of the nozzle device is to insert and attach the supply capillaries to the SGIC. The capillaries with an outer diameter of 360 μm have to be inserted into the receiving channels of the SGIC. These consist of a 170 μm deep trench in the silicon, topped with a semicircular cap of radius 250 μm. To ensure a robust mechanical connection, the capillary has to be inserted several millimeters into the receiving channels. This insertion length determines the minimum size of the microfluidic structure with the shallowest channels of 170 μm. Liquid was supplied to the nozzle by a Shimadzu high pressure liquid chromatograph (HPLC) LC-20AD. The volumetric liquid flows were measured and controlled by these HPLC. Helium gas was supplied by using a Parker self-relieving pressure regulator connected to a Bronkhorst EL-Flow gas mass flow meter.

For SFX experiments, it is beneficial that the nozzles can operate in air and in vacuum. Therefore, our tests included both environmental conditions. The performance tests of the hybrid nozzles were conducted in our laboratory under atmospheric conditions in a testing station already described in the work of Beyerlein *et al.*[23] When working in air, the gas-focused jets of various liquids were imaged using a Photron FASTCAM SA4 camera. The optics consisted of a Navitar Ultra-Zoom motorized lens, and the jets were illuminated by using a LDX Optronics 250 mW multi-mode fiber coupled to a 635 nm laser diode powered by a Newport LDP-3830 power supply. To image jets and droplets, a laser diode with 350 ns pulse duration was used. Measurements in a rough vacuum environment of 100 Pa were also carried out with an environmental scanning electron microscope (SEM, EVO MA 25, Carl Zeiss AG). To test the mechanical stability and to determine if there are any structural changes during the operation, we also imaged the internal structure of one nozzle after using it for several hours. This was done using X-ray radiography at 25 keV on beamline P05 PETRA III, DESY, Hamburg, Germany.

E. Jet characterization

The 3D printed nozzles as described above were tested under atmospheric conditions with gas and liquid parameters similar to those used in SFX experiments, e.g., with a water flow rate of 1-10 μl/min and a helium gas flow rate of 5-20 mg/min. Under these conditions, we obtained a minimum jet diameter of about 1.5 μm using our FASTCAM imaging setup. Indeed, all the tested nozzles had similar performance with minimum jet diameters of 1.5-2 μm [see Fig. 4(a)]. The 1.5 μm thick jet was about 90 μm long. Figure 4(b) shows an SEM image of a jet operating in vacuum, and Fig. 4(c) shows an X-ray radiograph of one nozzle. The radiograph was taken on a dry nozzle, after the experiment. Prior to this, the nozzle was producing a stable jet and was used for about 60 min (2-20 μl/min water and 2-20 mg/min He). The internal structure in Fig. 4(c) appears intact and as originally printed.

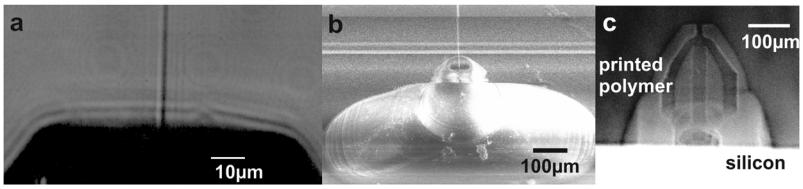

FIG. 4. SGIC-nozzle jet testing: (a) An image of a liquid jet propagating into the air from a nozzle on a SGIC. The jet diameter is approximately 1.5 μm. (b) An image of a liquid jet in vacuum at 100 Pa at higher flow rates. The jet diameter is about 5 μm. (c) An x-ray transmission image of a dry 3D printed nozzle on an SGIC.

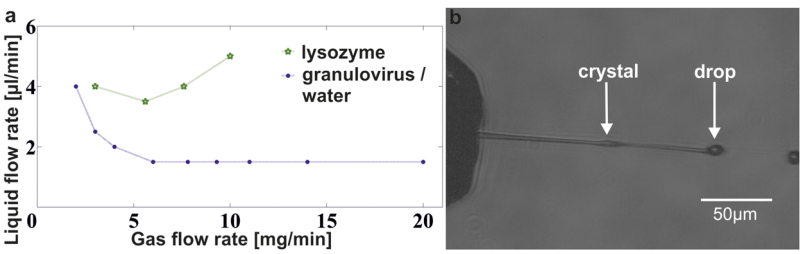

FIG. 5. Nozzle flow rate analysis: (a) Comparison of minimum flow rates in air required to create a jet of pure water (or buffer with granulovirus) and buffer with lysozyme. (b) About 5 μm diameter jet showing individual ~2 μm lysozyme crystals.

© Author(s) 2019

TABLE I. Maximum flow rate and pressure for nozzle bond strength test, SFX experiment, and smallest microjet with SGIC.

	Liquid lines		Gas lines	
	Max flow rate average (μl/min)	Applied average pressure (Pa)	Max flow rate average (mg/min)	Applied average pressure (Pa)
Nozzle with roots and seals	700	4.1×10^6	112	5.8×10^6
Nozzle with roots	362.5	3.2×10^6	100	5.5×10^6
Nozzle without roots and seals	300	2.6×10^6	86	4.8×10^6
Smallest microjet diameter with SGIC	1.5		6	
Standard SFX experiment	2-20	0.4×10^6-1.4×10^6	2-20	0.6×10^6-2.1×10^6

Since such nozzles are of interest for SFX experiments, we also performed tests with biological samples. We monitored the minimum flow rates of granulovirus and lysozyme crystals dispersed in liquid buffers and compared them with the flow rates of pure water. Lysozyme, also known as muramidase or *N*-acetylmuramide glycanhydrolase, is an antimicrobial enzyme produced by animals that forms part of the innate immune system. Granulovirus or *Cydia pomonella* granulosis virus is a virus of invertebrates, specifically the Codling moth, and used as a biological pesticide.

The minimum flow rates of pure water and the granulovirus were almost the same, which is not surprising because the size of the virus is very small, about 200 nm in diameter. The lysozyme crystals used in this study were about 2 μm in diameter and thus comparable to the diameter of the liquid jet. Thus, a higher liquid flow rate of 3.5-4 μl/min was required to form a stable jet, and under these conditions, the jet diameter was about 5 μm. The results are summarized in Fig. 5(a). In Fig. 5(b), the lysozyme crystals in the liquid jet can be clearly seen in an optical micrograph recorded with a 350 ns exposure time.

F. Bond connection test

To examine the connection between the nozzle and the substrate and to assess the bonding strength at high internal liquid and gas pressures, we performed a stress test. First, we tested the nozzles at low flow rates (below 10 μl/min water and 20 mg/min He). Any leakage or nozzle detachment observed at these low flow rates is most likely caused by the dirty silicon surface. Too short development time resulted in clogged nozzles, and bond connection tests were only performed on nozzles that jetted nicely at standard flow rates. For this, each nozzle was ramped up to as high a flow rate as possible, until it lost the connection and detached or formed a leak. We used capillaries with 360 μm outer and 150 μm inner diameter for the liquid and 100 μm inner diameter for the gas. These diameters are much larger than the inner diameters of capillaries usually used in SFX experiments (75 μm or 50 μm, respectively). Larger diameters of the supply lines require lower applied pressure to the liquid and gas entering the capillaries, here 1.5 m long, to achieve the flow rates needed to reach conditions of nozzle's failure.

The nozzles stayed attached to the substrates up to the maximum flow rates of 115 mg/min for He and 700 μl/min for water, which required input pressures of 5.5×10^6 Pa for the gas lines and 5.8×10^6 Pa for the liquid line (see results from a nozzle with roots and seals in Table I).

These rates are well beyond standard working conditions in SFX experiments, with typical flow rates of 2-20 mg/min for He and 2-20 μl/min for water.

We also tested the effectiveness of the root and seal structures on the nozzle's mechanical stability. In some nozzles, we removed only roots and in some both, seals and roots. Both types of nozzles could withstand the aforementioned high pressures and flow rates (Table I). However, the jets from nozzles without roots and seals were in general unstable, especially in the regime close to the maximum flow rate and before detachment or leakage occurred. Another peculiar difference between nozzles with and without root and seal structures was that nozzles with root and seal structure, which began leaking at flow rates above 100 μl/min, would continue to operate when the flow rate was reduced back to values of standard SFX flow rates. Under the same conditions, the nozzles without these structures detached from the SGIC. This demonstrates that the roots and seal structure are beneficial and increase the overall adhesion.

III. CONCLUSION

We demonstrated the feasibility of producing stable microjets using nozzles which were printed directly on microfluidic chips. Nozzles were 3D-printed by a two-photon polymerization process directly onto a microfluidic silicon glass interface chip. This printing enabled direct connections between the nozzle tip and gas and liquid channels and avoided extra steps that were previously required in the assembly of gas-focused liquid-jet nozzles used in serial diffraction experiments at X-ray free-electron laser sources. The precision obtained by direct printing in particular avoids the need to glue the capillaries to the nozzle tip, which had often led to misalignment, leaks, or clogging.

We report the details of the fabrication steps and the performance of 3D printed gas-dynamic virtual nozzles of a particular design. Under atmospheric conditions and 1.5 μl/min flow rate, these nozzles produced jets with a diameter of about 1.5 μm and a length of 90 μm. The chip production presented here is based on a standard silicon and glass technology, which allows fabrication of a fluidic platform with basic functions and integration of additional fluidic features. The GDVN was printed directly on the top of the silicon; this allows the exact, controlled, and reproducible fabrication of real 3D nozzles with a fast design and test cycle by rapid prototyping methods. The connection between the nozzle and chip is strong enough to allow significantly higher flow rates than what

© Author(s) 2019

is needed in typical serial crystallography experiments. Such hybrid technology combines silicon-glass microchips and 2-pp printing and opens a path to novel fluidic designs including sensing, sorting, and mixing.

ACKNOWLEDGMENTS

We thank Luigi Adriano (DESY) for technical assistance and Dr. Dominik Oberthür (DESY) for preparation of virus and lysozyme crystal samples used during the experiments. We thank Dr. Fabian Wilde and Dr. Jörg U. Hammel (both Helmoltz-Zentrum Geesthacht) for providing access to the P05 beamline and help with measurements and data evaluation of the x-ray radiograph. We also acknowledge the support of the Hamburg University of Technology and DESY Strategy Fund and the Deutsche Forschungsgemeinschaft (DFG) through the Gottfried Wilhelm Leibniz Program.

REFERENCES

[1]H. N. Chapman, P. Fromme, A. Barty, T. A. White, R. A. Kirian, A. Aquila, M. S. Hunter, J. Schulz, D. P. DePonte, U. Weierstall, R. B. Doak, F. R. N. C. Maia, A. V. Martin, I. Schlichting, L. Lomb, N. Coppola, R. L. Shoeman, S. W. Epp, R. Hartmann, D. Rolles, A. Rudenko, L. Foucar, N. Kimmel, G. Weidenspointner, P. Holl, M. Liang, M. Barthelmess, C. Caleman, S. Boutet, M. J. Bogan, J. Krzywinski, C. Bostedt, S. Bajt, L. Gumprecht, B. Rudek, B. Erk, C. Schmidt, A. Hömke, C. Reich, D. Pietschner, L. Strüder, G. Hauser, H. Gorke, J. Ullrich, S. Herrmann, G. Schaller, F. Schopper, H. Soltau, K. Kühnel, M. Messerschmidt, J. D. Bozek, S. P. Hau-Riege, M. Frank, C. Y. Hampton, R. G. Sierra, D. Starodub, G. J. Williams, J. Hajdu, N. Timneanu, M. M. Seibert, J. Andreasson, A. Rocker, O. Jönsson, M. Svenda, S. Stern, K. Nass, R. Andritschke, C. Schröter, F. Krasniqi, M. Bott, K. E. Schmidt, X. Wang, I. Grotjohann, J. M. Holton, T. R. M. Barends, R. Neutze, S. Marchesini, R. Fromme, S. Schorb, D. Rupp, M. Adolph, T. Gorkhover, I. Andersson, H. Hirsemann, G. Potdevin, H. Graafsma, B. Nilsson, and J. C. H. Spence, Nature **470**, 73 (2011).

[2]A. Barty, C. Caleman, A. Aquila, N. Timneanu, L. Lomb, T. A. White, J. Andreasson, D. Arnlund, S. Bajt, T. R. M. Barends, M. Barthelmess, M. J. Bogan, C. Bostedt, J. D. Bozek, R. Coffee, N. Coppola, J. Davidsson, D. P. DePonte, R. B. Doak, T. Ekeberg, V. Elser, S. W. Epp, B. Erk, H. Fleckenstein, L. Foucar, P. Fromme, H. Graafsma, L. Gumprecht, J. Hajdu, C. Y. Hampton, R. Hartmann, A. Hartmann, G. Hauser, H. Hirsemann, P. Holl, M. S. Hunter, L. Johansson, S. Kassemeyer, N. Kimmel, R. A. Kirian, M. Liang, F. R. N. C. Maia, E. Malmerberg, S. Marchesini, A. V. Martin, K. Nass, R. Neutze, C. Reich, D. Rolles, B. Rudek, A. Rudenko, H. Scott, I. Schlichting, J. Schulz, M. M. Seibert, R. L. Shoeman, R. G. Sierra, H. Soltau, J. C. H. Spence, F. Stellato, S. Stern, L. Strueder, J. Ullrich, X. Wang, G. Weidenspointner, U. Weierstall, C. B. Wunderer, and H. N. Chapman, Nat. Photonics **6**, 35 (2012).

[3]M. Gañán-Calvo, Phys. Rev. Lett. **80**, 285 (1998).

[4]U. Weierstall, Philos. Trans. R. Soc., B **369**, 20130337 (2014).

[5]D. P. DePonte, U. Weierstall, K. Schmidt, J. Warner, D. Starodub, J. C. H. Spence, and R. B. Doak, J. Phys. D: Appl. Phys. **41**, 195505 (2008).

[6]R. Zahoor, G. Belšak, S. Bajt, and B. Šarler, Microfluid. Nanofluid. **22**, 87 (2018).

[7]D. Oberthuer, J. Knoška, M. O. Wiedorn, K. R. Beyerlein, D. A. Bushnell, E. G. Kovaleva, M. Heymann, L. Gumprecht, R. A. Kirian, A. Barty, V. Mariani, A. Tolstikova, L. Adriano, S. Awel, M. Barthelmess, K. Dörner, P. L. Xavier, O. Yefanov, D. R. James, G. Nelson, D. Wang, G. Calvey, Y. Chen, A. Schmidt, M. Szczepek, S. Frielingsdorf, O. Lenz, E. Snell, P. J. Robinson, B. Šarler, G. Belšak, M. Maček, F. Wilde, A. Aquila, S. Boutet, M. Liang, M. S. Hunter, P. Scheerer, J. D. Lipscomb, U. Weierstall, R. D. Kornberg, J. C. H. Spence, L. Pollack, H. N. Chapman, and S. Bajt, Sci. Rep. **7**, 46846 (2017).

[8]G. Nelson, R. A. Kirian, U. Weierstall, N. A. Zatsepin, T. Faragó, T. Baumbach, F. Wilde, F. B. P. Niesler, B. Zimmer, I. Ishigami, M. Hikita, S. Bajt, S. Yeh, D. L. Rousseau, H. N. Chapman, J. C. Spence, and M. Heymann, Opt. Express **24**, 11515 (2016).

[9]M. O. Wiedorn, D. Oberthür, R. Bean, R. Schubert, N. Werner, B. Abbey, M. Aepfelbacher, L. Adriano, A. Allahgholi, N. Al-Qudami, J. Andreasson, S. Aplin, S. Awel, K. Ayyer, S. Bajt, I. Barák, S. Bari, J. Bielecki, S. Botha, D. Boukhelef, W. Brehm, S. Brockhauser, I. Cheviakov, M. A. Coleman, F. Cruz-Mazo, C. Danilevski, C. Darmanin, R. B. Doak, M. Domaracky, K. Dörner, Y. Du, H. Fangohr, H. Fleckenstein, M. Frank, P. Fromme, A. M. Gañán-Calvo, Y. Gevorkov, K. Giewekemeyer, H. M. Ginn, H. Graafsma, R. Graceffa, D. Greiffenberg, L. Gumprecht, P. Göttlicher, J. Hajdu, S. Hauf, M. Heymann, S. Holmes, D. A. Horke, M. S. Hunter, S. Imlau, A. Kaukher, Y. Kim, A. Klyuev, J. Knoška, B. Kobe, M. Kuhn, C. Kupitz, J. Küpper, J. M. Lahey-Rudolph, T. Laurus, K. Le Cong, R. Letrun, P. L. Xavier, L. Maia, F. R. N. C. Maia, V. Mariani, M. Messerschmidt, M. Metz, D. Mezza, T. Michelat, G. Mills, D. C. F. Monteiro, A. Morgan, K. Mühlig, A. Munke, A. Münnich, J. Nette, K. A. Nugent, T. Nuguid, A. M. Orville, S. Pandey, G. Pena, P. Villanueva-Perez, J. Poehlsen, G. Previtali, L. Redecke, W. M. Riekehr, H. Rohde, A. Round, T. Safenreiter, I. Sarrou, T. Sato, M. Schmidt, B. Schmitt, R. Schönherr, J. Schulz, J. A. Sellberg, M. M. Seibert, C. Seuring, M. L. Shelby, R. L. Shoeman, M. Sikorski, A. Silenzi, C. A. Stan, X. Shi, S. Stern, J. Sztuk-Dambietz, J. Szuba, A. Tolstikova, M. Trebbin, U. Trunk, P. Vagovic, T. Ve, B. Weinhausen, T. A. White, K. Wrona, C. Xu, O. Yefanov, N. Zatsepin, J. Zhang, M. Perbandt, A. P. Mancuso, C. Betzel, H. N. Chapman, and A. Barty, Nat. Commun. **9**, 4025 (2018).

[10]NanoscribeGmbH, user manual, https://www.nanoscribe.de/en/, 07, 2017.

[11]J. R. Stagno, Y. Liu, Y. R. Bhandari, C. E. Conrad, S. Panja, M. Swain, L. Fan, G. Nelson, C. Li, D. R. Wendel, T. A. White, J. D. Coe, M. O. Wiedorn, J. Knoska, D. Oberthuer, R. A. Tuckey, P. Yu, M. Dyba, S. G. Tarasov, U. Weierstall, T. D. Grant, C. D. Schwieters, J. Zhang, A. R. Ferré-D'Amaré, P. Fromme, D. E. Draper, M. Liang, M. S. Hunter, S. Boutet, K. Tan, X. Zuo, X. Ji, A. Barty, N. A. Zatsepin, H. N. Chapman, J. C. H. Spence, S. A. Woodson, and Y.-X. Wang, Nature **541**, 242 (2017).

[12]M. Trebbin, K. Krüger, D. DePonte, S. V. Roth, H. N. Chapman, and S. Förster, Lab Chip **14**(10), 1733 (2014).

[13]H. Y. Park, X. Qiu, E. Rhoades, J. Korlach, L. W. Kwok, W. R. Zipfel, W. W. Webb, and L. Pollack, Anal. Chem. **78**, 4465 (2006).

[14]A. M. Ross and J. Lahann, Annu. Rev. Chem. Biomol. Eng. **6**, 161 (2015).

[15]M. Iosin, T. Scheul, C. Nizak, O. Stephan, S. Astilean, and P. Baldeck, Microfluid. Nanofluid. **10**, 685 (2011).

[16]J. Wang, Y. He, H. Xia, L. Niu, R. Zhang, Q. Chen, Y. Zhang, Y. Li, S. Zeng, J. Qin, B. Lin, and B. Sun, Lab Chip **10**, 1993 (2010).

[17]J. Oever, N. Spannenburg, H. Offerhaus, D. Ende, J. Herek, and F. Mugele, J. Micro/Nanolithogr., MEMS, MOEMS **14**(2), 023503 (2015).

[18]B. Xu, Y. Zhang, H. Xia, W. Dong, H. Ding, and H. Sun, Lab Chip **13**, 1677 (2013).

[19]L. Amato, Y. Gu, N. Bellini, S. M. Eaton, G. Cerullo, and R. Osellame, Lab Chip **12**, 1135 (2012).

[20]M. H. Olsen, G. M. Hjortø, M. Hansen, Ö. Met, I. M. Svane, and N. B. Larsen, Lab Chip **13**, 4800 (2013).

[21]C. Gati, D. Oberthuer, O. Yefanov, R. D. Bunker, F. Stellato, E. Chiu, S. Yeh, A. Aquila, S. Basud, R. Bean, K. R. Beyerlein, S. Botha, S. Boutet, D. P. DePonte, R. B. Doak, R. Fromme, L. Galli, I. Grotjohann, D. R. James, C. Kupitz, L. Lomb, M. Messerschmidt, K. Nass, K. Rendek, R. L. Shoeman, D. Wang, U. Weierstall, T. A. White, G. J. Williams, N. A. Zatsepin, P. Fromme, J. C. H. Spence, K. N. Goldie, J. A. Jehle, P. Metcalf, A. Barty, and H. N. Chapman, Proc. Natl. Acad. Sci. U. S. A. **114**, 2247 (2017).

[22]K. R. Beyerlein, D. Dierksmeyer, V. Mariani, M. Kuhn, I. Sarrou, A. Ottaviano, S. Awel, J. Knoska, S. Fuglerud, O. Jönsson, S. Stern, M. O. Wiedorn, O. Yefanov, L. Adriano, R. Bean, A. Burkhardt, P. Fischer, M. Heymann, D. A. Horke, K. E. J. Jungnickel, E. Kovaleva, O. Lorbeer, M. Metz, J. Meyer, A. Morgan, K. Pande, S. Panneerselvam, C. Seuring, A. Tolstikova, J. Lieske, S. Aplin, M. Roessle, T. A. White, H. N. Chapman, A. Meentsa, and D. Oberthuer, IUCrJ **4**, 769 (2017).

[23]K. R. Beyerlein, L. Adriano, M. Heymann, R. Kirian, J. Knoška, F. Wilde, H. N. Chapman, and S. Bajt, Rev. Sci. Instrum. **86**, 125104 (2015).

© Author(s) 2019